RSC Advances

ROYAL SOCIETY OF CHEMISTRY

www.rsc.org/advances

Deep Adsorption Desulfurization of Liquid Petroleum Gas by Copper-Modified Bentonite

Qian Zhang, Li Shi, and Xuan Meng*

The State Key Laboratory of Chemical Engineering, East China University of Science and Technology, Shanghai 200237, People's Republic of China.

ABSTRACT: In this paper, the removal of sulfur compounds from LPG has been investigated by using a fixed-bed flow sorption system. The modified bentonite adsorbents significantly enhanced the desulfurization ability of LPG. Several factors which influence the desulfurization capability, including loading, baking temperature, valence state and types of copper compounds were investigated. The adsorbents were characterized by nitrogen adsorption, X-ray diffraction (XRD), inductively coupled plasma−atomic emission spectrometer (ICP-AES), thermal analysis (TGA), raman spectroscopy and FT-IR spectroscopy. The experiment results showed that the Cu(II) modified bentonite adsorbents had optimum desulfurization ability with loading 15wt% Cu^{2+} and calcination temperature at 150 °C. In addition, the Cu(I) modified bentonite is better than Cu(II) modified bentonite adsorbents in removal sulfur compounds from LPG, and anion to the desulfurization ability of Cu(II) modified bentonite adsorbents had no significant influence. The Lewis acid sites contributed to the desulfurization were obtained via FT-IR analyses. The Raman analyses indicated that sulfur compounds were adsorbed over Cu(I)-bentonite and Cu(II)-bentonite by a direct S-adsorbent (S-M) interaction.

Keywords: Bentonite; LPG; desulfurization; modified; copper

1. INTRODUCTION

Liquid Petroleum gas (LPG) is one of the top products of the crude distillation at refineries and consists mainly of light hydrocarbon compounds. Liquid petroleum gas is not only the main household fuels in many cities and towns all over the world, especially in China, but also as petrochemical feed stock. The isobutylene from LPG is mainly used for the production of methyl tertiary butyl ether (MTBE), which is a kind of high-quality high octane number gasoline added components. The physical properties of the MTBE and the gasoline hydrocarbons are similar, therefore, it has good miscibility with gasoline and without phase separation occurs even though in any proportion immiscible. MTBE not only can improve the gasoline octane number,

* To whom correspondence should be addressed. E-mail: mengxuan@ecust.edu.cn Tel.: 021-64252383.

and can also make gasoline composite more reasonable through indirectly reduce sulfur, olefins, aromatics content and vapor pressure of gasoline. Sufficient use of C4 hydrocarbon from LPG is significant to improve the economic benefits and provide additional value. However, the LPG from fluid catalytic crack or delayed coking process usually contain various kinds of sulfur compounds, including carbonyl sulfide (COS) , mercaptan, carbon disulfide (CS_2) , dimethyl sulfide (DMS) , and dimethyl disulfide (DMDS) , and so forth.[1,2] Generally, among the organic sulfur compounds, DMS and DMDS are the most difficult to remove because of their poor reactivity and polarity.[3] Therefore, it is necessary to remove these sulfur compounds in a pretreatment process before synthesis MTBE since they result in high sulfur content of subsequent products and poisoning of catalysts.

In fact, before 2010, the U.S. environmental protection agency (EPA) had already issued regulations that the total sulfur content must be less than10 ppmw in gasoline.[2] Similar regulations were implemented in some cities of China in 2012, such as: Beijing, Shanghai.[4] Sulfur-free fuel has been a goal in all countries across the world. For the purpose, various desulfurization processes, including hydrodesulfurization (HDS), selective catalytic oxidation (SCO) and adsorptive desulfurization (ADS), are being carried out remove sulfur compounds from commercial fuels. In these conventional removals of sulfur compounds, the HDS processes have been most extensively applied to reduce sulfur levels from commercial fuels. However, HDS is not suitable for desulfurization of LPG. There are two reasons following about it. On the one hand , HDS processes using Co−Mo/Al_2O_3, Ni−Mo/Al_2O or Ni–W/Al_2O_3 as catalysts and be operated at high temperature (300−400 °C) and pressure (20−100 atm of H_2) conditions;[5,6] On the other hand, also is the most important reason, HDS processes is difficult to meet the current sulfur level requirements.[7] Furthermore, during the desulfurization process, loss of olefin may be significant because of the conversion of paraffin.[8, 9] The same, the SCO process also leads to waste of olefins because of oxidation and polymerization of olefins. Therefore, alternative processes that could achieve sulfur removal without significant loss of octane index are investigated.[10] Contrary to the above processes, ADS process has the advantages that it does not require hydrogen addition and can be operated at ambient conditions. It also has strengths of flexibility, low energy, safety and operation cost.[11, 12]

ADS is regarded as one of the most competitive methods for desulfurization, especially for ultra-deep desulfurization of fuels. Deep desulfurization on various adsorbents such as activated carbons (ACs), [2, 13-15] modified composite oxide,[16]

zeolite[1,17,18] , mesoporous silicas,[19,20] and metal-organic frameworks,[21,22] have already been studied. There are some different ways of remove sulfur compounds. Yang and co-workers[23-25] reported the adsorptive desulfurization of transportation fuels over Ag^+ and Cu^+ ion exchanged Y zeolites. They attributed the good desulfurization performance of adsorbents to π-complexation. Song et al.[26] reported that sulfur compounds can be selectively removed through direct sulfur−adsorbent (S−M) interaction. Although considerable research has been devoted to the desulfurization of liquid transportation fuels, few studies have been reported on the deep desulfurization of LPG.

Recently, Takatsu et al.[17] have studied the removal of DMDS, DMS, COS, TBM in LPG. They have used activated carbon, ZnO/Al_2O_3, Ag-exchanged β-zeolite and Ag/CeO_2. Among the tested adsorbents, Ag-exchanged β-zeolite and Ag-exchanged β-zeolite showed better adsorption capacity than others for sulfur compounds like DMDS, DMS, and TBM. They have deduced that the electrostatic attraction between the Ag-exchanged β-zeolite and sulfur compounds played a critical role in the adsorption of sulfur compounds by comparing the charge of sulfur atom on each molecule.

In recent decades, bentonite is increasingly attracting widespread attention as a new type of mesoporous materials that can serve as separating agents or sorbents, due to its excellent physical and chemical properties, which are high specific surface area, low cost, ordered structure, thermal stability, high exchange capacity and adsorptive affinity for organic and inorganic ions.[27] In this paper, the main objective of this research is to study the efficiency of modified bentonite for various organic sulfur compounds in LPG through using a dynamic adsorption method in a fixed bed. The adsorbents were characterized by nitrogen adsorption, X-ray diffraction (XRD), inductively coupled plasma−atomic emission spectrometer (ICP-AES), thermal analysis (TGA), Raman spectroscopy and FT-IR spectroscopy.

2. EXPERIMENTAL SECTION

2.1. Materials and feedstocks. In this paper, the raw activated bentonite was obtained from Zhejiang Province, China. The composition of the bentonite is presented in Table 1.

The Liquid Petroleum gas was obtained from delayed coking process of the oil Quanzhou refinery (Fujian Province, China). The composition of the LPG is presented in Table 2.

2.2. Adsorbent Preparation. The procedures of adsorbent preparation were as

follows. Firstly, the activated bentonite and with different content $Cu(NO_3)_2$ were mixed completely in a mixing kneader. Then, a moderate amount of deionized water was added to the mixture to make the slurry. Secondly, the raw materials, which had been mixed through stirring for a period of time, were sent to the extruder to squeeze into the form of strips to make a series of modified bentonite. Thirdly, the moisture of the extrudate was removed in an oven at 120 °C in a 4 h drying process. Finally, the extrudate was baked in a muffle furnace at 150 °C in air for 2 h, then crushed and screened to 20−40 mesh. $CuBr_2$-bentonite, $CuSO_4$-bentonite and $CuCl_2$-bentonite were prepared by the same method. The preparation method of CuCl-bentonite only the last step is different from the above methods. The CuCl-bentonite sample was baked at 150 °C for 2 h in pure N_2.

2.3. Adsorption Desulfurization Experiments. Evaluation of the adsorption desulfurization performance of sorbents was carried out in a fixed-bed flow sorption system with a stainless steel column (8 mm I.D.(internal diameter)×400mm length). The adsorbent particles were packed into the middle of the column and the remaining space were filled with quartz sand. The experiments were conducted under the following conditions: 0.6 MPa and room temperature, liquid hourly space velocity (LHSV) 10.0 h^{-1}. The concentration of sulfur compounds was analyzed hourly after each test started at the inlet and outlet. The outflow total sulfur compounds contents were analyzed by ultraviolet fluorescence sulfur nitrogen analyzer. A breakthrough sulfur content was defined as the effluent concentration of sulfur reaches 5 $mg.m^{-3}$. The desulfurization capacity was calculated by the following equation:

$$S_t = \frac{q \times 10^{-6} \times 100\%}{m} \int_0^t (C_0 - C_t)dt$$

where S_t is the amount of sulfur adsorbed on the adsorbent (wt% mg-S/g of adsorbent), q is the flow velocity of the LPG (ml/h), C_0 is the inlet sulfur concentration of the LPG (mg/m^3), and C_t is the outlet sulfur concentration of the LPG (mg/m^3) at any time t (h), and m is the mass of the adsorbent (g).

2.4. Characterization of adsorbents. *2.4.1. Power X-ray Diffraction (XRD).* The crystalline structure of the adsorbents was confirmed by power X-ray diffraction by using a Siemens D–500 X–ray diffractometer equipped with Ni–filtrated CuK_α radiation (40 kV tube voltage, 100 mA tube current and λ=0.154nm). The 2θ scanning angle range was 5–80° in a step of 0.02°/s. The crystallite size of samples was calculated from XRD patterns with Sherrer formula:

$$d = \frac{0.89\,\lambda}{\beta \cos\theta}$$

Where d is the crystallite size, λ is the wavelength of X-ray and β is the width at the half maximum of diffraction peak.

2.4.2. Nitrogen Isotherms. The BET specific surface area of bentonite were measured by nitrogen adsorption at –196 °C using a micromeritics (JW-BK112). Prior to analysis, the samples were degassed for 2h at 120 °C under a vacuum of $P<10^{-2}$ Pa to a constant pressure. The specific BET surface areas were determined from the N_2 adsorption at relative pressures of $0.05 < P/P_0 < 0.35$. The pore size distribution (PSD) was obtained from the adsorption branch of the N_2 sorption isotherms using the Barret–Joyner–Halenda (BJH) formula.[28] The total pore volumes (V_t) were estimated from the volume of N_2 (as liquid) held at a relative pressure (P/P_0) of 0.99.

2.4.3. ICP-AES. The actual copper loading amount in $Cu(NO_3)_2$-bentonite adsorbents was tested by an inductively coupled plasma−atomic emission spectrometer (ICP-AES) Agilent 725ES analyzer.

2.4.4. Thermal Analysis. The thermal gravimetric analysis is important techniques used to distinctly show the effect of thermal stability of the solid materials. Thermo-gravimetric (TG) curves were recorded by using a TA Instruments thermal analyzer. The sample was ground to 200 mesh. This work was measured at air atmosphere and at a heating rate of 10 °C/min in the temperature range 25-700 °C.

2.4.5. FT-IR Spectroscopy. Using pyridine as the probe molecule, the type and number of the adsorbents' surface acidity were tested by Fourier transform infrared (FT–IR) spectroscopy. Firstly, the sample loaded in the in-site cell was pretreated to remove the moisture at 380 °C under vacuum condition. Secondly, excess of pyridine adsorption after cooling down to 80 °C. Finally, the adsorbed pyridine were desorbed at 200 °C and 450 °C for 2 h.

2.4.6. Raman spectroscopy. The Raman spectra studies were conducted on a Renishaw System 100 Raman spectrometer using 514 nm red excitation from an Ar laser. The laser power was 3 mW at the sample position. The Raman scattered light was detected perpendicular to the laser beam with a Peltiercooled CCD detector, and the spectral resolution in all measurements was 1 cm^{-1}.

3. RESULTS AND DISCUSSION

3.1. XRD characterizations of the adsorbents. X–ray diffraction analysis in Figure 1 and 2 were carried out in order to identify the mineralogical structure of the modified bentonite adsorbents. As shown in Figure 1 and 2, the XRD pattern of the adsorbents showed SiO_2 of bentonite characteristic reflections at 2θ=20.81° and

26.61°. In other words, structure of bentonite remained intact after modified. However, the crystallinities of the modified bentonite adsorbents slightly decreased compared to raw-bentonite, due to the framework defects caused by the loading metal ion.

As can be seen from Figure 1, XRD patterns of the $CuBr_2$-bentonite samples examined at the big angle showed the characteristic reflections for $CuBr_2$ species at 2θ=27.06°, 44.97° and 53.27° corresponding to the planes (002), (110) and (112) of cubic $CuBr_2$ species, respectively. The characteristic reflections for $CuSO_4{\cdot}5H_2O$ species at 2θ =16.09°, 18.70°, 22.17° and 23.93° corresponding to the (110), (011), (101) and (111) planes, respectively, indicating that the cubic structure of $CuSO_4{\cdot}5H_2O$ species. XRD patterns of the $CuCl_2$-bentonite samples show the characteristic reflections for $CuCl_2$ species at 2θ=16.27°, 22.96° and 40.89°corresponding to the (101), (110) and (011) planes, respectively, which is indicative of a cubic phase. For the CuCl-bentonite samples, the Cu_2O diffraction peak at 2θ of 16.14° can be indexed to the (111) reflection of cubic Cu_2O species. The calculated mean particle size of the loaded $CuBr_2$, $CuSO_4{\cdot}5H_2O$, $CuCl_2$ and Cu_2O particles by Scherrer equation were about 60, 59, 110 and 38 nm (which corresponds the strongest peak of (002), (011) , (101) and (111)), respectively.

In Figure 2, XRD patterns of the $Cu(NO_3)_2$-bentonite samples show the characteristic reflections for $Cu_2(OH)_3NO_3$ species at 2θ=12.74° and 25.76° corresponding to the (001) and (002) planes of cubic $Cu_2(OH)_3NO_3$ species, respectively, which is attributed to the incomplete decomposition of trace $Cu(NO_3)_2$. [18] And the weak peak of CuO observed at 2θ values of 33.52 can be indexed to the (211) reflection of cubic CuO species, which is due to the partial oxidation of $Cu(NO_3)_2$. The average crystallite size of $Cu_2(OH)_3NO_3$ and CuO species are calculated to be 130 and 41nm using the Scherrer formula (which corresponds the strongest peak of(001) and (211)). Furthermore, the $Cu_2(OH)_3NO_3$ peaks of the modified bentonite adsorbents increased gradually with the copper loading increased.

3.2. Nitrogen Isotherms. Figure 3 and 4 show the N_2 adsorption-desorption isotherms and pore size distribution curves of raw-bentonite and $Cu(NO_3)_2$- bentonite with different copper loading. All samples exhibit type IV isotherms with capillary condensation step and a strong peak on the pore size distribution curves, which are characteristic of mesoporous materials according to the IUPAC classification.[29]

Table 3 depicts structural parameters of the adsorbents from Nitrogen Adsorption Isotherms. As shown in table 3, the BET surface area, pore size and total pore volume decreased with the increase of cuprum ion loading for $Cu(NO_3)_2$-bentonite adsorbents,

the raw-bentonite adsorbent had the biggest BET surface area, pore size and total pore volume. The decrease in the BET surface area, pore size and total pore volume might be due to the deposition of metal cluster onto the surface of the channels of bentonite.[30] In addition, these modified bentonite adsorbents haven't the same BET surface area and total pore volume even though loading same metal ion on bentonite. The BET surface area was in "$Cu(NO_3)_2$-bentonite > CuCl-bentonite > $CuBr_2$-bentonite > $CuCl_2$-bentonite > $CuSO_4$-bentonite" order. The total pore volume in "$Cu(NO_3)_2$-bentonite > CuCl-bentonite > $CuCl_2$-bentonite > $CuBr_2$-bentonite > $CuSO_4$-bentonite" order.

3.3. Effects of different cupric compound on adsorption desulfurization of LPG. In order to examine the effect of different cupric compound on adsorption desulfurization of LPG, four modified bentonite adsorbents were prepared by using the mixed method. As shown in Figure 5, except for the $CuCl_2$-bentonite adsorbent, others adsorbents were observed to have almost the same ability of remove sulfur, but the difference was small. Therefore, we could confirmed that anion to the desulfurization ability of Cu(II) modified bentonite adsorbents had no significant influence. Combined with Table 3, the active order of adsorbents had no corresponding relation between BET surface area and total pore volume. The result indicated that Cu^{2+} played a critical role to ADS of LPG rather than anion.

Because of the almost same activity of adsorbents, the following research on modified component content we choose copper nitrate.

3.4. Effects of the amount of Cu^{2+} loading on desulfurization performance. Dynamic tests were carried out to examine the effect of the loading amount of copper on desulfurization performance, four $Cu(NO_3)_2$-bentonite adsorbents with different copper loading amount of 5, 10, 15 and 20 wt% were prepared by using the mixed method. Figure 6 shows the experimental results on $Cu(NO_3)_2$ modified bentonite adsorbents. As shown in Figure 6, compared to raw bentonite adsorbent, the modified adsorbents could remove sulfur for longer time. In addition, at the low $Cu(NO_3)_2$ concentrations, the sulfur removal level of the adsorbents increased with the increasing of the $Cu(NO_3)_2$ concentration. When the amount of $Cu(NO_3)_2$ loading was 15 wt%, the sulfur removal level reached optimum. However, in the case of 20 wt% $Cu(NO_3)_2$-bentonite, the sulfur removal level decreased obviously. As shown in table 3, compared to raw bentonite adsorbent, the modified adsorbents' total pore volume and the BET surface area were decreased. However, the performance of modified adsorbents were still higher than raw-bentonite. This result can be explained by the

chemical interaction force between the sulfur compounds and the $Cu(NO_3)_2$ content of the adsorbents. However, the sulfur removal level decreased obviously when the $Cu(NO_3)_2$ concentration was above a certain threshold due to the extra metal cluster may jam the pore channels of the adsorbents and block off the active sites. This indicates that there are some trade-off effects between the amount of loading $Cu(NO_3)_2$ and the sulfur removal level. Therefore, the sulfur removal level can be controlled by choosing an appropriate concentration of the $Cu(NO_3)_2$ for LPG.

3.5. Effects of baking temperature on adsorption desulfurization of LPG. Different baking temperatures from 120 ℃ to 350 ℃ were measured with 15 wt% $Cu(NO_3)_2$-bentonite adsorbent. The results were exhibited in Figure 7. As shown in Figure 7, the baking temperature has a strong effect on adsorption desulfurization of LPG, from 150 ℃ to 350 ℃, the sulfur removal ability of adsorbents were gradually reduced. And the optimal baking temperature of 15 wt% $Cu(NO_3)_2$-bentonite adsorbent was 150 ℃.

In order to show the effect of thermal stability of the adsorbents, the thermal analysis was carried out. The DSC–TGA curves for raw-bentonite and 15 wt% $Cu(NO_3)_2$-bentonite adsorbents were shown in Figures 8. From the DTG curve of raw adsorbent, the peak in the range of 25-150 ℃ represents the water adsorbed in the bentonite. However, from the DTG curve of 15 wt% $Cu(NO_3)_2$-bentonite, the first peak was centered at 25-150 ℃ represents the water adsorbed in the bentonite. The second peak in the range of 200-300 ℃ was caused by the decomposition of $Cu(NO_3)_2$.[18] As shown in Figure 7, the ADS performance of absorbent baked at 150 ℃ was better than which baked at 120 ℃, because the water would block the pores of the adsorbent.

In order to analyze the actual decomposition products of $Cu(NO_3)_2$ under the different baking temperature, the power X-ray diffraction was carried out. As shown in Figure 9, the results indicated that the decomposition products of $Cu(NO_3)_2$ were $Cu_2(OH)_3NO_3$ and CuO at baking temperature of 120 ℃ and 150 ℃. However, the decomposition products of $Cu(NO_3)_2$ were CuO at baking temperature of 250 ℃ and 350 ℃. Combined with Figure 6, the ADS performance of absorbent baked at 150 ℃ was better than which baked at 250 ℃ and 350 ℃, the results indicated that $Cu_2(OH)_3NO_3$ plays a more dominant role than CuO for the removal of sulfur compounds in the LPG.

3.6. Performance of Cu(II) and Cu(I) on adsorption desulfurization of LPG. In the following research, we investigated that the performance of valence of copper on

adsorption desulfurization of LPG, and $CuCl_2$-bentonite and CuCl-bentonite were prepared. As shown in Figure 10, Cu(I)-bentonite exhibited better removal of sulfur ability than Cu(II)-bentonite.

The surface acidic sites of Cu(II) and Cu(I)–bentonite adsorbents were tested by FT–IR spectra for the adsorption of pyridine at 200 °C and 450 °C . As shown in Figure 11 and 12, it shows Lewis as well as Brønsted acidity in these samples. The band at 1540 cm^{-1} was assigned to Brønsted acid sites whereas the band at 1450cm^{-1} was assigned to Lewis acid sites. As shown in Figure 11, the characteristic peaks at 1450cm^{-1} arising from the vibrations of pyridine molecules adsorbed at Lewis acid sites for the modified bentonite adsorbents. It is evident that Cu(I) and Cu(II)-bentonite adsorbents show higher Lewis acidity compared to the raw-bentonite adsorbent, because of the metal cations electron acceptors. In addition, it indicated that the total number of Lewis acid sites on the surface of Cu(I)–bentonite was more than Cu(II)–bentonite. As can be seen in Figure 12, strong Lewis acid sites only present on the Cu(I)–bentonite adsorbent. The higher Lewis acidity facilitates the Cu(I)–bentonite to adsorption of sulfur compounds that are electron donors. So we concluded that the total number of Lewis acidity of the adsorbents facilitates adsorption of sulfur compounds from LPG.

Yi et al.[31] reported that sulfur compounds can be removed through direct S-M interaction. The Raman spectrum of Cu(I)-bentonite and Cu(II)-bentonite the adsorbents after adsorption sulfur compounds of LPG were shown in Figure 13. The two peaks at 286 cm^{-1} and 416 cm^{-1} were observed in curve a, however, only one peak at 280 cm^{-1} was observed in curve b. These regions are characteristic of the Cu-S stretching vibrations,[32] indicating that sulfur compounds are adsorbed over Cu(I)-bentonite and Cu(II)-bentonite by a direct S-adsorbent (S-M) interaction.

4. CONCLUSIONS

The copper modified bentonite were excellent adsorbents for the remove of sulfur compounds from LPG. The report confirmed that anion to the desulfurization ability of Cu(II) modified bentonite adsorbents had no significant influence. The bentonite loaded with 15 wt% copper and calcinated at 150 °C showed an optimal sulfur adsorption ability in the desulfurization of LPG containing about 29.4$mg.m^{-3}$ sulfur. In addition, the Cu(I) modified bentonite is better than Cu(II) modified bentonite adsorbents in remove sulfur compounds from LPG. The Lewis acid sites contributed to the desulfurization were obtained via FT-IR analyses. The Raman analyses indicated that sulfur compounds are adsorbed over Cu(I)-bentonite and

Cu(II)-bentonite by a direct S-adsorbent (S-M) interaction.

ACKNOWLEDGMENTS

This work is financially supported by the National Natural Science Foundation of China (No. 21276086).

REFERENCES

[1] Lee. J, Beum. H. T, Ko. C. H, Park. S. Y, Park. J. H, Kim.J.N, Chun. B. H and Kim. S. H, *Ind. Eng. Chem. Res.* 2011, **50**, 6382−6390.

[2] Kim. K. S, Park. S. H, Park. K. T, Chun. B. H and Kim. S. H, *Korean J. Chem. Eng.* 2010, **27**, 624−631.

[3] Crespo. D, Qi. G, Wang. Y, Yang. F. H and Yang. R. T, *Ind. Eng. Chem. Res.* 2008, **47**, 1238−1244.

[4] Li. D, *Chin. J. Catal.* 2013, **34**, 48−60.

[5] Hernández-Maldonado. A. J and Yang. R. T, *Catal. Rev.* 2004, **46**, 111−150.

[6] Herna´ndez-Maldonado. A. J and Yang. R. T, *Ind. Eng. Chem. Res.* 2004, **43**, 1081−1089.

[7] Babich. I. V and Moulijn. J. A, *Fuel* 2003, **82**, 607-631.

[8] Wang. L, Li. S, Cai. H, Xu. Y, Wu. X and Chen. Y, *Fuel* 2012, **94**, 165−169.

[9] Wang. Y, Yang. R. T and Heinzel. J. M, *Chem. Eng. Sci.* 2008, **63**, 356−365.

[10] Song. C, *Catal. Today* 2003, **86**, 211−263.

[11] Duan. L, Gao. X, Meng. X, Zhang. H, Wang. Q, Qin. Y, Zhang. X and Song. L, *J. Phys. Chem. C.* 2012, **116**, 25748−25756.

[12] Shahadat Hussain. A. H. M and Tatarchuk. B. J, *Fuel* 2012, **107**, 465−473.

[13] Yahia A. A and Hisham S. B, *Fuel* 2009, **88***,* 87–94.

[14] Tang. X. L, Qian. W, Hu. A, Zhao. Y. M, Fei. N. N and Shi. L, *Ind. Eng. Chem. Res.* 2011, **50**, 9363−9367.

[15] Cui. H, Turn. S. Q and Reese. M. A, *Catal. Today* 2009, **4**, 274−279.

[16] Sentorun-Shalaby. C, Saha. S. K, Ma. X. L and Song. C. S, *Appl. Catal. B.* 2011, **101**, 718−726.

[17] Takatsu. K, Takegoshi. G, Katsuno. H, Kawashima. Y and Matsumoto. H, *J. Jpn. Pet. Inst.* 2007, **4**, 200−207.

[18] Le. C. S, Ting. T. B, Li. J. Z, Yu. L. Z, Yu. Z. X and Dao. H. X, *Phys. Chem. C.* 2014, **118**, 9468−9476.

[19] Yin. Y, Xue. D. M, Liu. X. Q, Xu. G, Ye. P, Wu. M. Y and Sun. L. B, *Chem. Commun.* 2012, **48**, 9495−9497.

[20] Tan. P, Qin. J. X, Liu. X. Q, Yin. X. Q and Sun. L. B, *J. Mater. Chem. A,* 2014, **2**,

4698−4705.

[21] Hasan. Z and Jhung. S. H, *ACS Appl. Mater. Interf.* 2015, **7**, 10429−10435.

[22] Li. Y. X, Jiang. W. J, Tan. P, Liu. X. Q, Zhang. D.Y and Sun. L. B, *J. Phys. Chem. C.* 2015, **119**, 21969-21977.

[23] Yang. R. T., Hernández-Maldonado. A. J and Yang. F. H, *Science* 2003, **301**, 79−81.

[24] Hernández-Maldonado. A. J and Yang. R. T, *J. Am. Chem. Soc.* 2004, **126**, 992−993.

[25] Hernández-Maldonado. A. J and Yang. R. T. *Ind. Eng. Chem. Res.* 2003, **42**, 123−129.

[26] Velu. S, Ma. X and Song. C, *Ind. Eng. Chem. Res.* 2003, **42**, 5293−5304.

[27] Tang. X. L, Meng. X and Shi. L, *Ind. Eng. Chem. Res.* 2011, **50**(12), 7527−7533.

[28] Barrett. E. P, Joyner. L. J and Halenda. P. P, *J. Am. Chem. Soc.* 1951, **73**, 373–380.

[29] Sing. K. S. W, Everett. D. H, Haul. R. A. W, Moscou. L, Pierotti. R. A, Rouquérol. J and Siemieniewska. T, *Pure Appl. Chem.* 1985, **57**, 603−619.

[30] Kaur. J, Griffin. K, Harrison. B and Kozhevnikov. I. V, *J. Catal.* 2002, **208**, 448-455.

[31] Yi. D. Z, Huang. H, Meng. X and Shi. L, *Appl. Catal. B.* 2014 ,**148**, 377–386.

[32] Colin. R. A, Hyeyeong Y, Joan. S. V, Gdran. K. B, Nicklas. B, Gertie. V. P, Gerard. W. C, Thomas. M. L and Joann. S. L, *J. Am. Chem. SOC.* 1994, **116**, 11489–11498.

Table 1. Composite of Lin An Activated Bentonite.

Components	Content(wt%)
SiO_2	67.8
Al_2O_3	16.3
Na_2O	0.9
Fe_2O_3	4.0
CaO	1.1
K_2O	1.6
MgO	2.1
others	7.0

Table 2. Compositions of LPG.

Name	Content (wt%)	S concentration($mg.m^{-3}$)
Paraffin	**77.5**	
N-butane	24.1	
Iso-butane	14.2	
Propane	39.2	
Olefin	**14.2**	
Proplyene	3.9	
Butylene	10.3	
Others	8.3	
Total	100	
Sulfur compound		**29.94**
Carbonyl sulfide		7. 32
Carbon disulfide		0. 67
Dimethyl disulfide		7. 45
Methanethiol		10.66
Ethanethiol		3.42
Hydrogen sulfide		0.42

Table 3. Structural Parameters of the Adsorbents from Nitrogen Adsorption Isotherms

Sample	Actual Cu content (wt%)	BET surface area (m^2/g)	Vtotal (cm^3/g)	BJH pore size (nm)
Raw bentonite	0	179.212	0.294	8.615
5wt% $Cu(NO_3)_2$-bentonite	4.6	138.681	0.262	6.584
10wt% $Cu(NO_3)_2$-bentonite	9.6	127.106	0.243	6.341
15wt% $Cu(NO_3)_2$-bentonite	14.5	107.754	0.223	5.915
20wt% $Cu(NO_3)_2$-bentonite	19.2	108.037	0.232	5.854
15wt% $CuCl_2$-bentonite	14.1	77.037	0.203	7.762
15wt% $CuSO_4$-bentonite	14.5	70.526	0.165	7.212

15wt% $CuBr_2$-bentonite	14.6	93.987	0.192	6.446
15wt% CuCl-bentonite	14.6	93.995	0.213	7.546

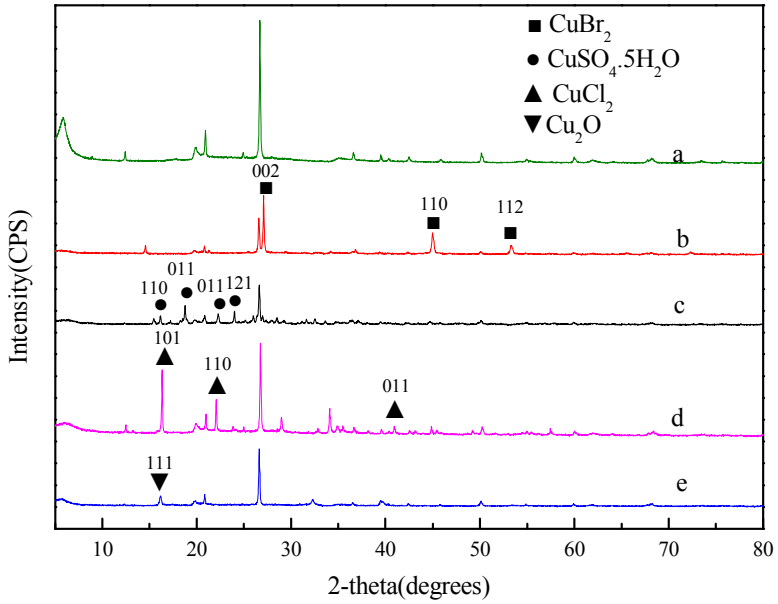

Figure 1. X-ray diffraction patterns of Cu-bentonite with different copper compound: (a) raw-bentonite, (b) $CuBr_2$-bentonite, (c) $CuSO_4$-bentonite, (d) $CuCl_2$-bentonite, (e) CuCl-bentonite.

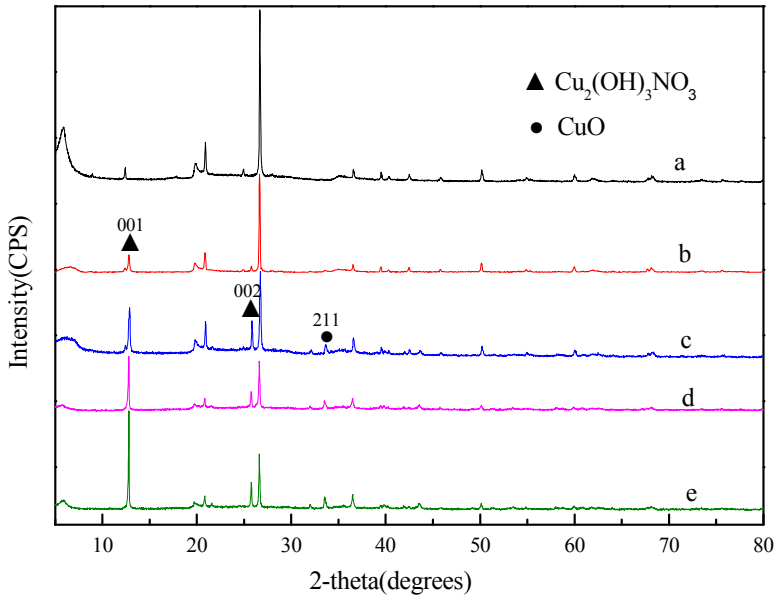

Figure 2. X-ray diffraction patterns of Cu-bentonite with different copper content: (a) raw-bentonite, (b) 5 wt%, (c) 10 wt%, (d) 15 wt%, (e) 20 wt%.

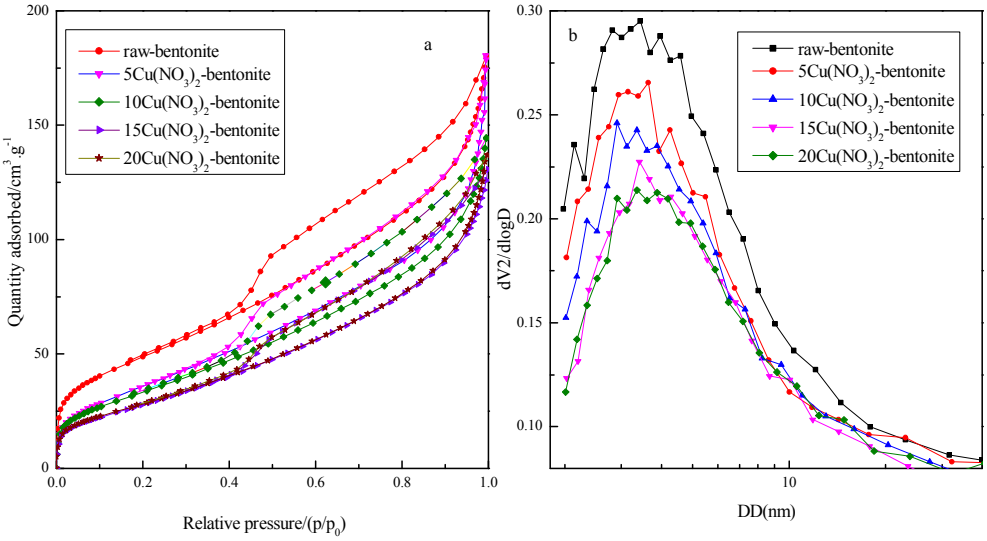

Figure 3. (a) N_2 adsorption-desorption isotherms and (b) pore size distribution curves of raw-bentonite and $Cu(NO_3)_2$- bentonite with different copper loading.

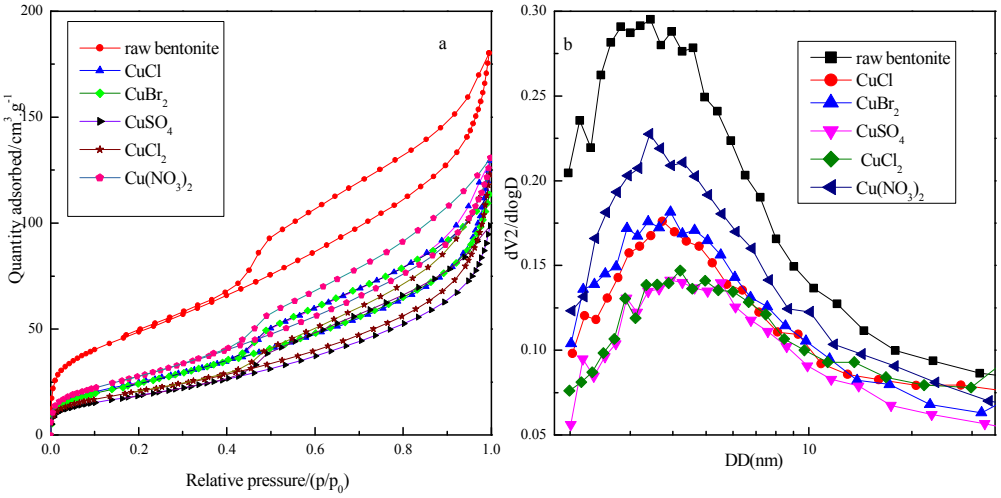

Figure 4. (a) N_2 adsorption-desorption isotherms and (b) pore size distribution curves of raw-bentonite and bentonite with different copper compound.

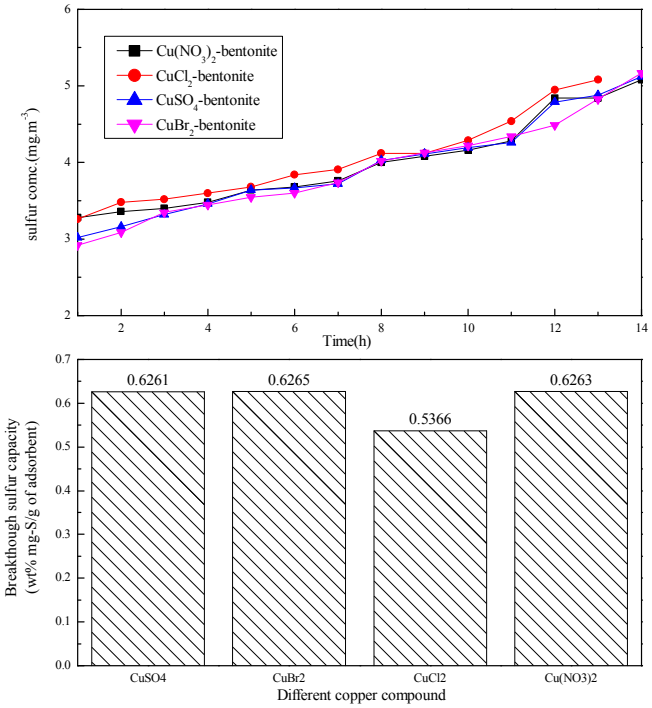

Figure 5. Breakthrough curves and sulfur capacities of ADS over loading different copper compound on bentonite.

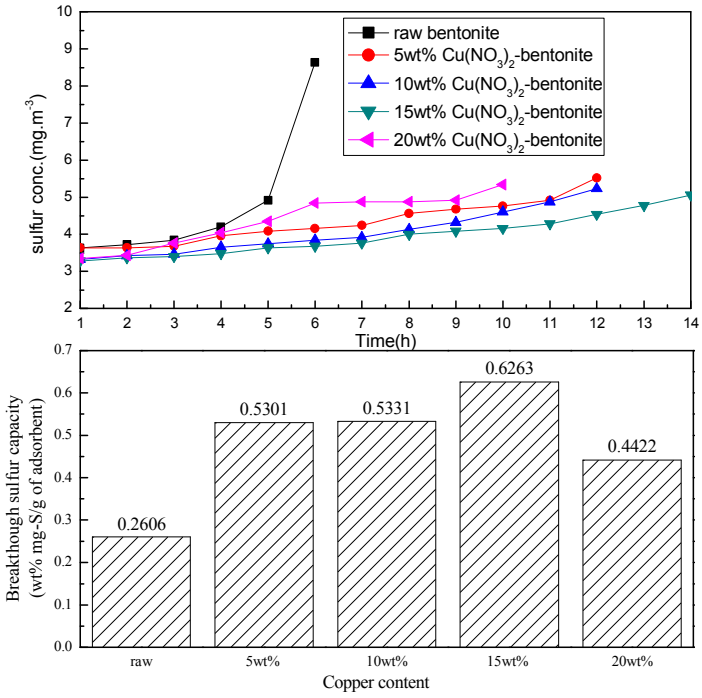

Figure 6. Breakthrough curves and sulfur capacities of ADS over $Cu(NO_3)_2$-bentonite sorbents

with different copper loading.

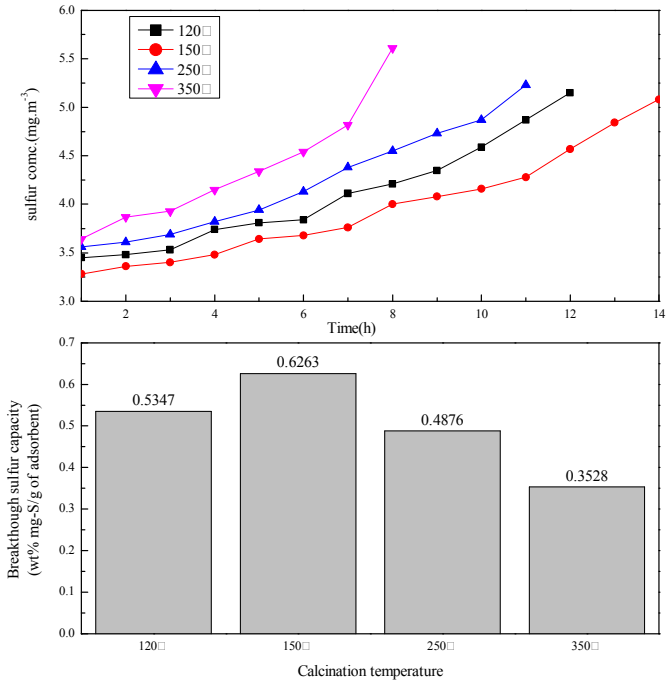

Figure 7. Breakthrough curves and sulfur capacities of ADS with different baking temperature of 15 wt% $Cu(NO_3)_2$-bentonite.

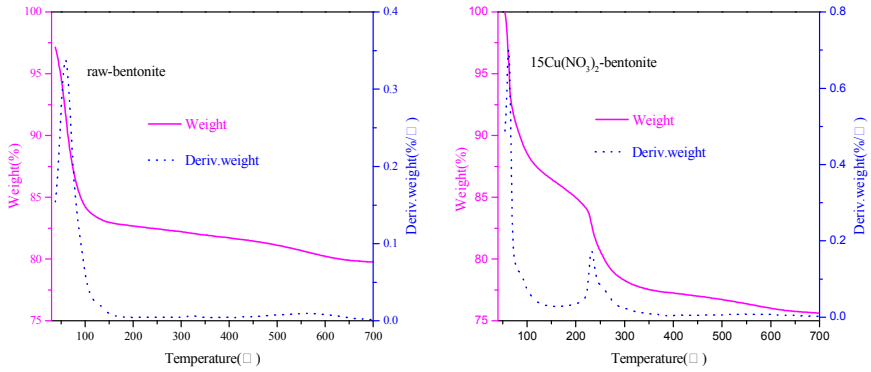

Figure 8. DSC-TGA curves in air for the raw-bentonite and 15 wt% $Cu(NO_3)_2$-bentonite.

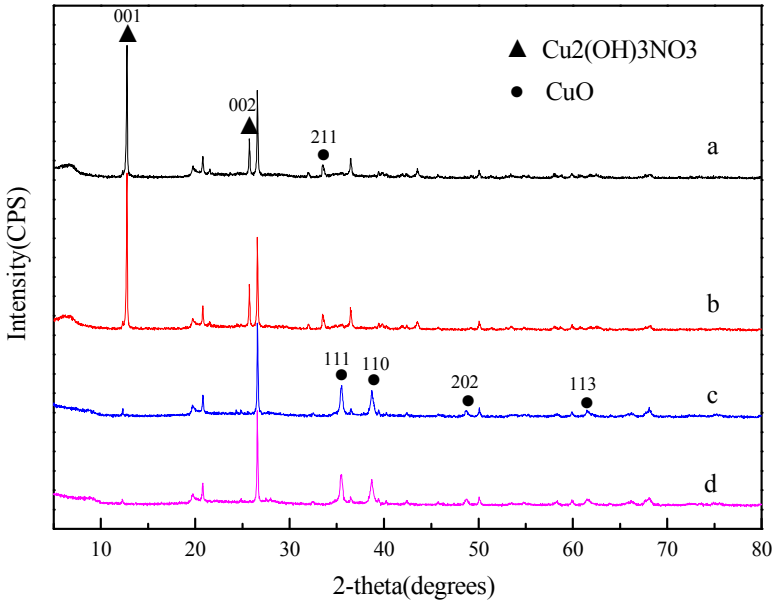

Figure 9. X-ray diffraction patterns of 15 wt% $Cu(NO_3)_2$-bentonite with different baking temperature: (a)120 °C, (b) 150 °C, (c) 250 °C, (d) 350 °C.

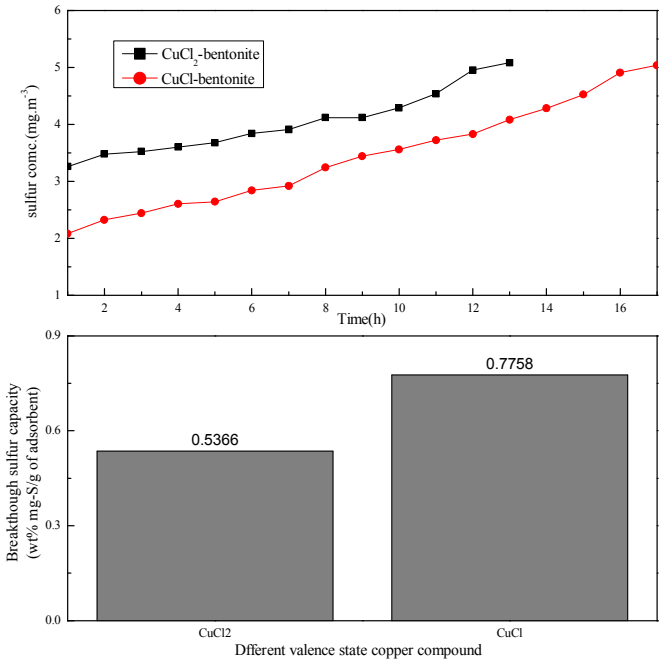

Figure 10. Breakthrough curves and sulfur capacities of ADS over Cu(II) and Cu(I) modified bentonite adsorbents.

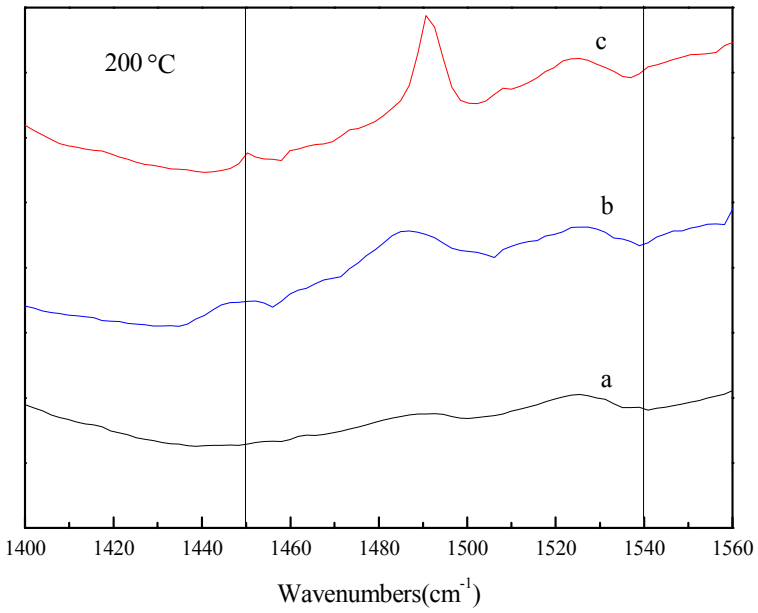

Figure 11. Pyridine FT–IR spectra of three adsorbents at 200 °C: (a)raw-bentonite; (b) Cu(I)–bentonite; (c) Cu(II)–bentonite.

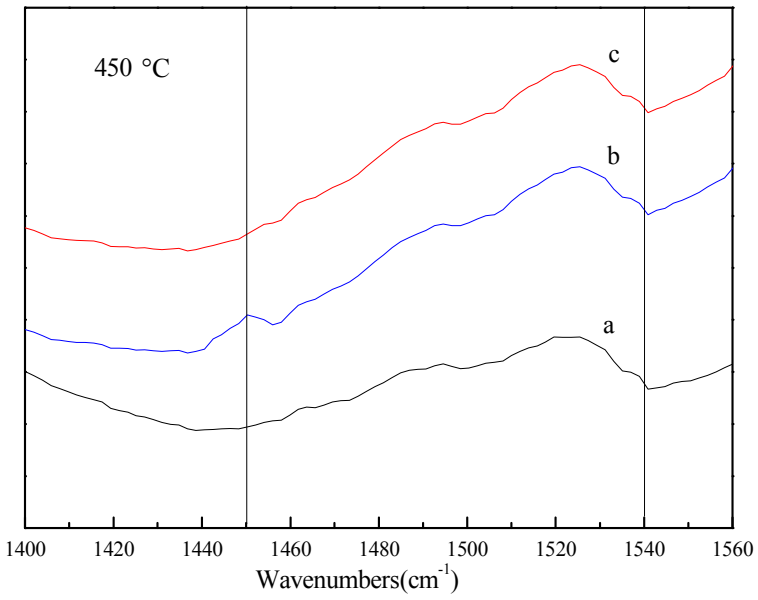

Figure 12. Pyridine FT–IR spectra of three adsorbents at 450 °C: (a) raw-bentonite; (b) Cu(I)–bentonite; (c) Cu(II)–bentonite.

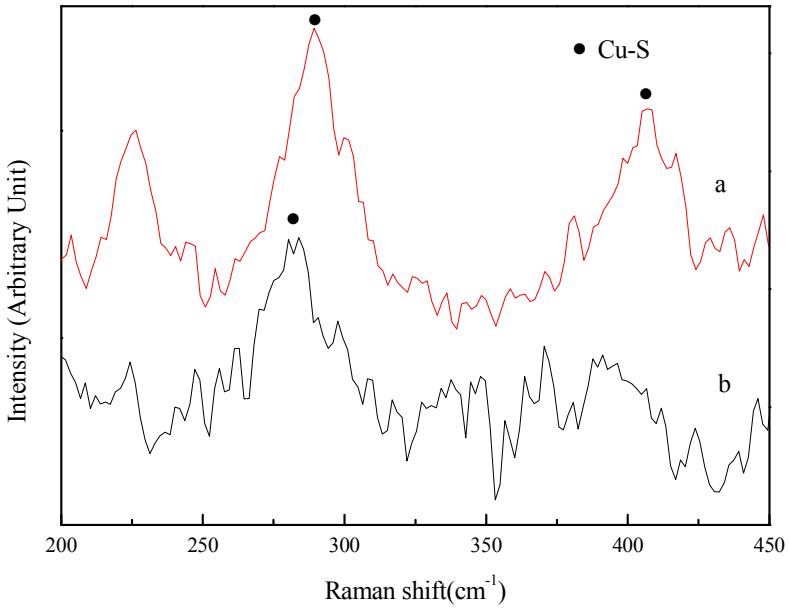

Figure 13. The Raman spectrum of the adsorbents: (a) CuCl-bentonite after adsorption of sulfur compounds in LPG, (b) $CuCl_2$-bentonite after adsorption of sulfur compounds in LPG.

Effects of the different cupric compound, amount of Cu^{2+} loading, baking temperature and valence state of copper on adsorption desulfurization of LPG.